EUROPEAN ORGANIZATION FOR NUCLEAR RESEARCH

CERN – AB DIVISION

Werner.Herr@cern.ch

Aperture and stability studies for the CNGS proton beam line TT41

W. Herr and M. Meddahi, AB Division, CERN, 1211-Geneva 23

Abstract

The aim of this study is to check by means of simulations the aperture of the CNGS proton beam line, and to investigate the beam stability in position and angle at the target.

Geneva, Switzerland

1st March 2003

1 CNGS proton beam

The CERN neutrinos to Gran Sasso (CNGS) project, presently under construction, is a collaboration between CERN and the Gran Sasso Laboratory in Italy, with the aim to study neutrino oscillations in a long base-line experiment [1, 2, 3]. An intense proton beam is extracted from the SPS accelerator at a nominal energy of 400 GeV, transported through a 840 m long proton transfer line, before impinging on a graphite target. Secondary particles created in the target are directed towards Gran Sasso and will, in turn, decay in flight, producing muon-type neutrinos. These neutrinos, which hardly interact with matter, will travel 730 km through the earth towards the Gran Sasso laboratory, where the appearance of tau-type neutrinos will be studied. The general CNGS layout is shown in Fig.1. The proton beam

Figure 1: *Overview of the CNGS Layout.*

is extracted from the SPS in LSS4 at 400 GeV, in two consecutive 10.5 μs fast extractions, in a 6 s cycle. The nominal intensity per extraction is 2.4 10^{13} p/extraction with an upgrade phase to 3.5 10^{13} p/extraction. The CNGS proton beam will be using the same fast extraction channel as the LHC beam in LSS4, and both beams are finally injected into a common beam line (TT40) of about 200 m [4, 5, 6, 7]. In order to steer this intense beam through the CNGS proton beam line (called TT41), beam position monitors and dipole correctors are positioned along the line. Trajectory optimisation has been performed and is documented in [9].

2 Vacuum chamber definition

The aperture types and dimensions used at the different elements in the beam line are given in Tab.1.

element	aperture type	horizontal aperture [mm]	vertical aperture [mm]
Dipole MBG	rectangle	81	34.5
Dipole MBHC	rectangle	152	34
Dipole MBHA	circle	49	
Dipole MBSG	rectangle	129	52.3
Quadrupole QTGF	ellipse	59.4	42.4
Quadrupole QTGD	ellipse	42.4	59.4
Quadrupole QTSF	ellipse	121	63
Quadrupole QTLF	ellipse	121	63
Quadrupole QTSD	ellipse	63	121
Quadrupole QTLD	ellipse	63	121
Quadrupole QTR	ellipse	62.35	62.35
Corrector MDSH	rectangle	152	59.5
Corrector MDSV	rectangle	59.5	152
Corrector MDGH	ellipse	75	40
Corrector MDGV	ellipse	40	75
Corrector MDMH	ellipse	45.36	29
Corrector MDMV	ellipse	29	65.5
BTV	circle	60	
BPM	circle	60	
BPCK	circle	133	
BFCT	circle	156	

Table 1: *Physical aperture of the proton beam line elements. The full heights and widths are given for rectangular and elliptical apertures and the diameter for circular apertures.*

3 Simulation program

All simulations are done with the newly developed MAD-X program [8]. The tracking is done using a thin lens version of the lattice. The particles are assigned initial coordinates and momenta in six dimensional phase space and tracked through each element of the beam line. The coordinates at the start and end of the line are always provided, but observation points can also be defined at any position in the line. MAD-X allows to assign a physical aperture to each element (as defined in Tab.1) and during tracking a particle is considered lost whenever its trajectory exceeds the aperture. This removes the need to place a collimator next to every element to do tracking with aperture restrictions, contrary to what had to be done with MAD8. No aperture limit was assigned to driftspaces and the MAD-X default (1 m) is used. Furthermore, the apertures can be misaligned, independent of the associated beam line elements, simulating a further restriction of the available space. For example, aperture at a quadrupole could be reduced by displacing its vacuum chamber while leaving the magnet aligned. Some of the magnets (type MBG) are tilted and the tracking is following the reference path.

In order to analyse the output from MAD-X and perform various calculations at all positions recorded (e.g. beam size and position), a post-processing program was written. This program also allows to plot the results obtained.

4 Check of available aperture

To check the available aperture, a set of particles at the beginning of the TT41 line have been generated and tracked through the elements using the MAD-X program. The position and angle of all particles at the start of the beam line and at the target, as well as at other observation points, are stored for post processing.

4.1 Tracking with initial phase space distribution

Tab.2 gives the Twiss parameters at the beginning of the beam line and at the target location. We have generated the particles according to a Gaussian distribution to follow the contour of the emittance ellipse. The nominal physical emittance is 28 nm, but in the following tracking studies, during the beam generation, an emittance 4 times larger was used in order to fill a larger part of the phase space. In this way the tails of the beam distribution are better populated. The phase space plots at the beginning of

	β_x (m)	β_x (m)	α_x	α_y	D_x (m)
Beginning of line:	18.932	111.892	0.674	-3.433	-0.393
End of line:	10.000	10.000	0.0	0.0	0.0

Table 2: *Twiss parameters at beginning of the TT41 line and at the target.*
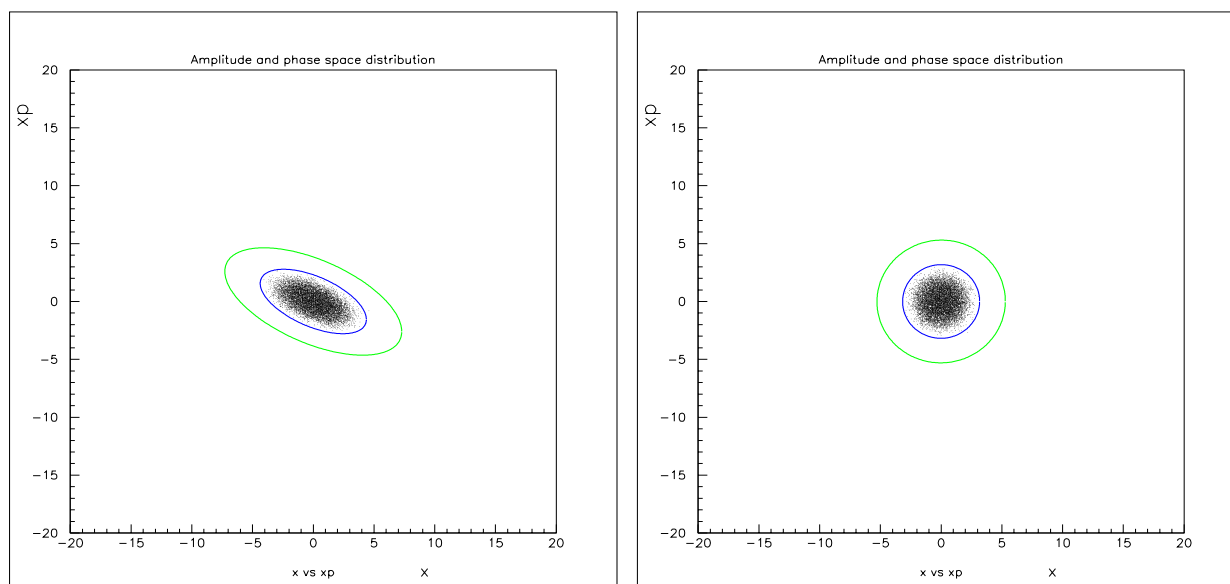
Figure 2: *Horizontal phase space at beginning of the beam line (left) and at the target (right). Units: 1 mm for the horizontal and 0.1 mrad for the vertical axis.*

the beam line and at the target are shown in the Figs.2 - 3. The circular or elliptical lines indicate the contour of 6 σ and 10 σ, respectively. The energy spread of the particles is taken as 0.06% r.m.s, which is close to the expected value. Units: 1 mm for the horizontal and 0.1 mrad for the vertical axis. No particle loss is observed, confirming that the initial design of the beam line was correct. During this first tracking study, no aperture displacement was applied.
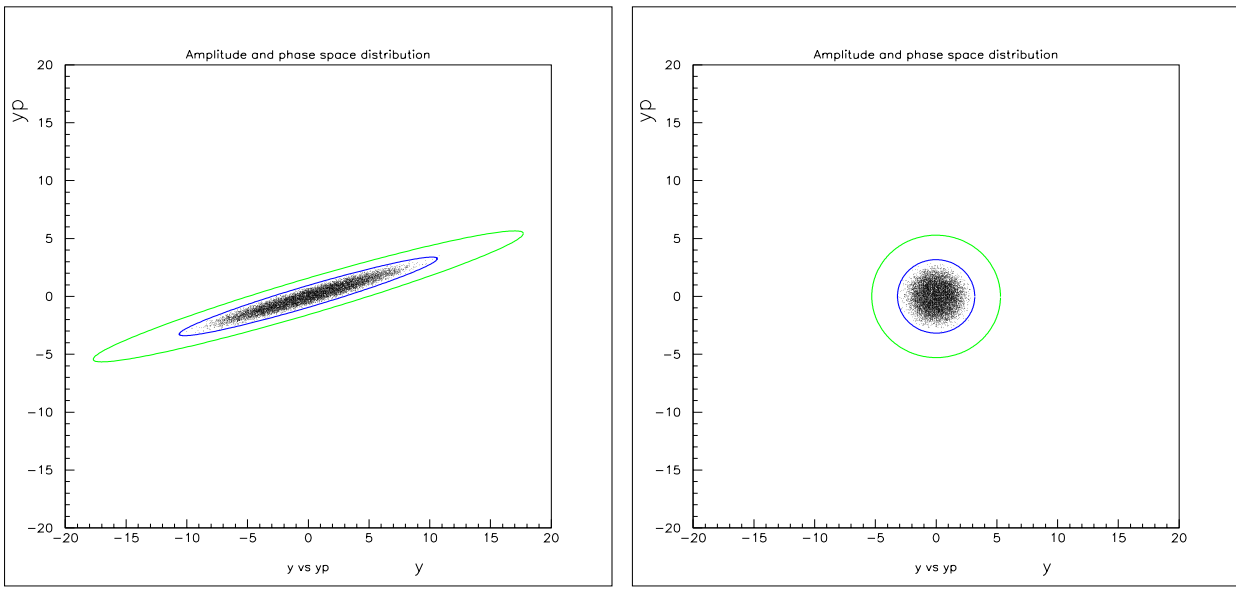
Figure 3: *Vertical phase space at beginning of the beam line (left) and at the target (left). Units: 1 mm for the horizontal and 0.1 mrad for the vertical axis.*
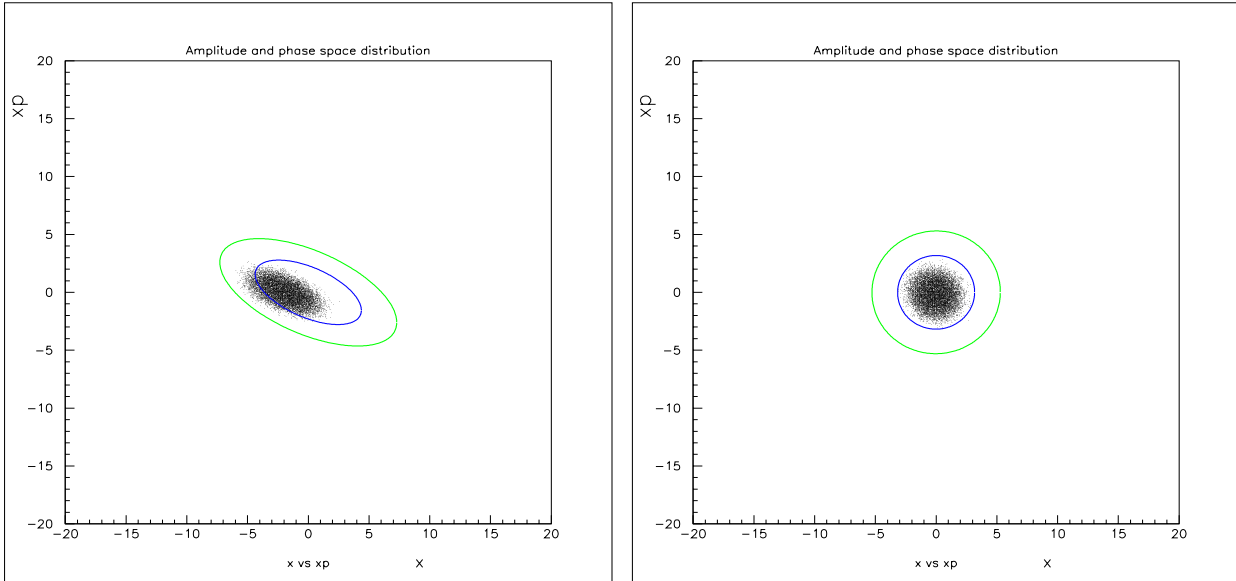
Figure 4: *Horizontal phase space at beginning of the beam line (left) and at the target (right). Momentum offset of 0.5%. Units: 1 mm for the horizontal and 0.1 mrad for the vertical axis.*

In Fig.4, in order to study the effect of a momentum offset, we tracked a set of particles with $\frac{\Delta p}{p} = 0.005$. Since the horizontal dispersion is non-zero at the beginning of the line, the horizontal position has to be slightly displaced in order to be centred again at the target. This is shown in Fig.4. We have tracked 100000 particles with different sets of momentum offset and aperture displacements and give the results in Tab.3. We show the fraction of lost particles. For an aperture displacement of ± 4.0 mm (expected uncorrected trajectory displacement [9]), and for a momentum offset of $\frac{\Delta p}{p} = 0.0015$ (expected 2 σ value [10]), no particle was lost for the initial distributions described above.

5

	±0.0 mm (m)	±1.0 mm (m)	±2.0 mm (m)	±4.0 mm (m)	±8.0 mm (m)
$\frac{\Delta p}{p} = 0.0000$	0.0	0.0	0.0	0.0	0.009
$\frac{\Delta p}{p} = 0.0010$	0.0	0.0	0.0	0.0	0.015
$\frac{\Delta p}{p} = 0.0015$	0.0	0.0	0.0	0.0	0.018
$\frac{\Delta p}{p} = 0.0050$	0.0007	0.004	0.013	0.085	0.563

Table 3: *Fraction of particles lost for different aperture misalignments and momentum offsets. 100000 particles were tracked through the TT41 line.*

4.2 Tracking with initially uniform distribution

We have also tracked particles with initially uniform distributions, occupying much more than the available aperture at entry. The phase space distributions at the end of the beam line for the horizontal and
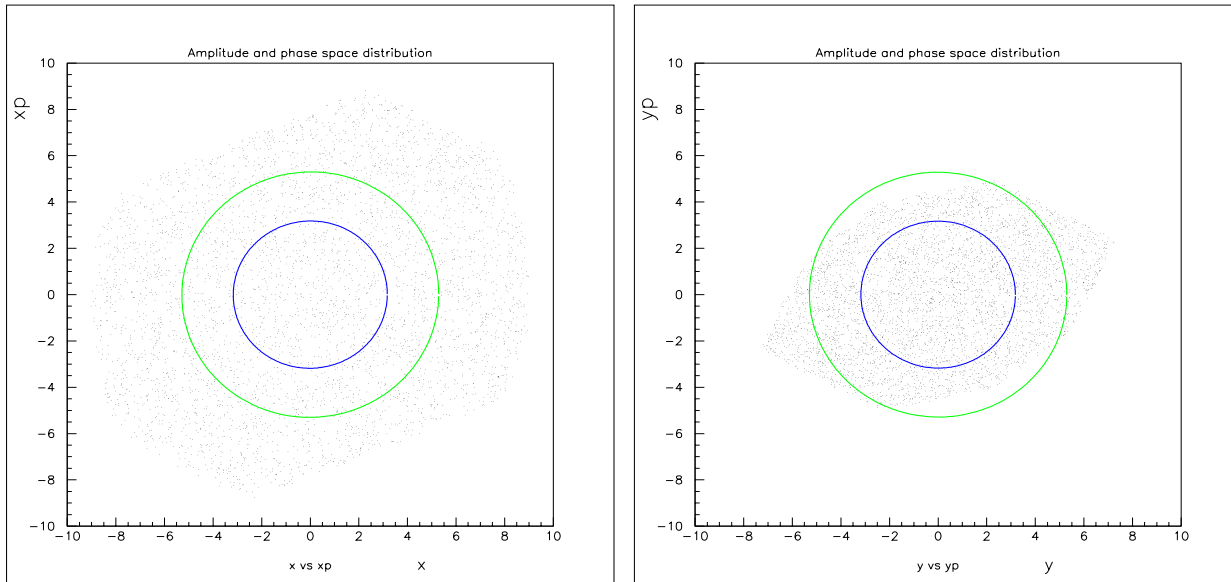
Figure 5: *Horizontal and vertical phase space at the target. Initial distribution flat. Units: 1 mm for the horizontal and 0.1 mrad for the vertical axis.*

vertical plane are shown in Fig.5 for 100000 particles generated. Most particles are lost at the very beginning of the beam line and the shape of the aperture limit in the line is clearly visible in Fig.5. For both planes the amplitudes of particles reaching the end of the line exceed the 6 σ contour significantly and confirm the earlier findings. The difference between the horizontal and vertical distribution is due to the scraping at the first (defocusing) quadrupole and the smaller vertical aperture of the dipole magnets. These dipole magnets with a full vertical aperture of 34 mm limit the available vertical aperture.

5   Beam stability on the target

The beam stability on the target is of great importance and we have evaluated the range of possible movement from extraction to extraction.

5.1   Imperfections

The following imperfections where included in the tracking program:

5.1.1   Injection errors:

The SPS beam is horizontally extracted from the SPS in the long straight section 4 using a fast extraction channel. Horizontal closed orbit bumpers, extraction kickers and DC electromagnetic septum magnets are the main ingredients of this extraction channel. The beam is moved close to the extraction septum using a horizontal closed orbit bump, and is then kicked horizontally across the septum, with the kicker field rising during a gap in the circulating SPS beam [11]. The extraction septum then deflects the beam out of the SPS vacuum chamber and into the transfer line TT40 with the required position and angle. We later refer to errors in this position and angle at the start of the TT40 line, as injection errors. Injection errors which can not be corrected, thus changing from extraction to extraction, are originating from the magnets of this SPS extraction channel. They were evaluated in [6] and are again taken to be Gaussian with a horizontal injection position error with a σ of 0.5 mm and a horizontal injection angle error with a σ of 0.01 mrad, both cut at $\pm$ 2 σ.

5.1.2   Main dipole (MBG, MBGT) field error:

There are 73 main dipole magnets in the line for which field dipole errors will contribute to a deviation from the reference trajectory. The specification requires that each magnets stays within $\pm$ 5.0 10^{-4} of the average field [12]. The resulting distribution of the deflections is assumed to be Gaussian with a σ of 2.0 μrad cut at $\pm$ 2 σ, which corresponds approximately to $\pm$ 5.0 10^{-4} of the nominal deflection of 8 mrad. Design field errors in the dipoles of other type (MBHC, MBHA, MBSG) are neglected as only few magnets of these types are used in the line, compared to the 75 main dipole magnets MBG in this single pass transfer line.

5.1.3   Main dipole tilt errors:

Magnet distortions around the beam axis (i.e. the direction of the field lines varies along the magnet length) are possible and should be taken into account. This tilt results in additional vertical deflections depending on the tilt angle whereas the normal horizontal deflection stay almost unchanged. During alignment, the resolution of each measurement done along the magnet to measure its tilt will be 0.2 mrad. For our simulations, the tilt errors are assumed to be distributed like a Gaussian with a σ of 1.6 μrad (0.2 mrad·8 mrad nominal horizontal deflection), cut at $\pm$ 4 σ.

5.1.4   Main quadrupole (QTG) errors:

All main quadrupoles (QTG, [13]) may experience in the tunnel unwanted displacement in the horizontal and vertical plane. These displacements are approximated by a Gaussian distribution with a σ of 0.2 mm. This distribution is cut at $\pm$ 3 σ. The origin of these displacements can come from the resolution during the alignment, and the deformation of the ground.

5.1.5   Dipole power supply precision:

The precisions of the power supplies are summarized in Tab.4.

Dipoles	nominal field [mrad]	power supply precision	field error [μrad]	1σ (2σ cut)[μrad]
MBG(T)	8	$\pm\, 2 * 10^{-5}$	0.16	0.08
MBHC	4.5	$\pm\, 10^{-4}$	0.45	0.225
MBHA	3.7	$\pm\, 10^{-4}$	0.37	0.185
MBSG	3.2	$\pm\, 10^{-4}$	0.32	0.16

Table 4: *Dipole power supply errors*

5.1.6 Quadrupole power supply precision

The following errors where taken for the quadrupole power supplies, as summarized in Tab.5.

Quadrupole	Maximum field [T/m]	power supply precision
QTGF	40	$\pm\, 10^{-4}$
QTGD	40	$\pm\, 10^{-4}$
QTSF/QTLF	24	$\pm\, 10^{-4}$
QTSD/QTLD	24	$\pm\, 10^{-4}$
QTR	47	$\pm\, 10^{-4}$

Table 5: *Quadrupole power supply errors*

These errors will result in optical errors in the beam line. We assume that the beginning of the beam line is matched to the SPS optics at the extraction point.

5.2 Strategy for tracking

In the previous section we have introduced two types of errors: those which can fluctuate from extraction to extraction such as instability of the power supplies, and others which we assume to be constant with time, such as misalignments of beam line elements.

For the simulation we have started a particle (representing a bunch) at the beginning of the beam line and tracked it through the lattice with both static misalignments and other errors allowed to change from extraction to extraction (for each particle tracked), according to the above specifications (such as power supply ripple). The trajectory due to misalignments is assumed to be corrected to a reasonable degree so
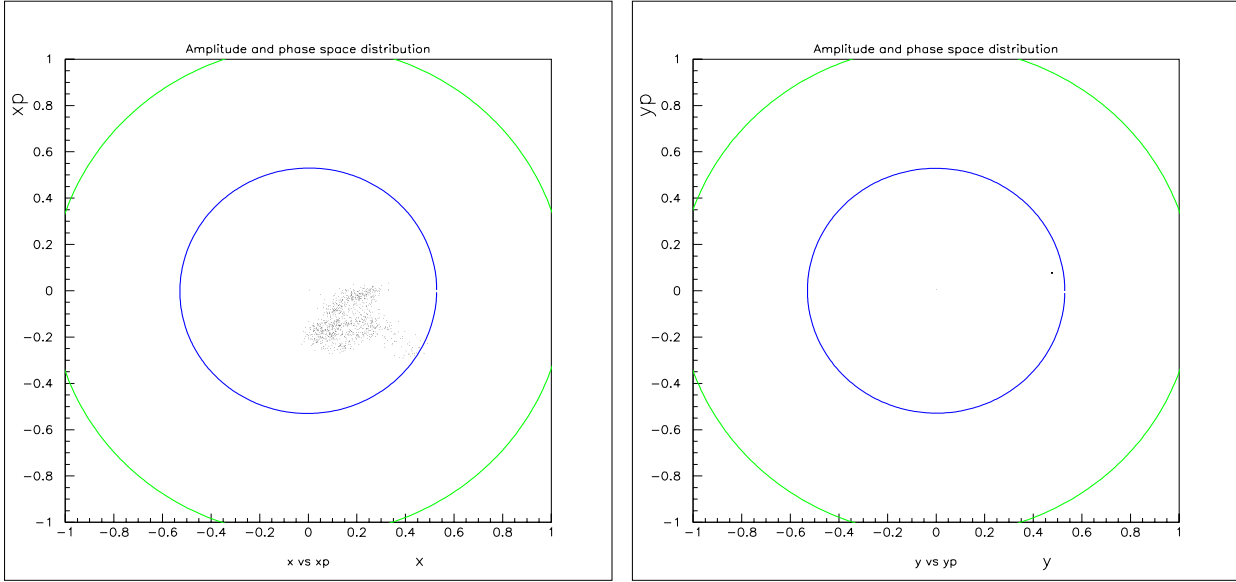
Figure 6: *Stability and beam spot at the target. Left figure horizontal and right figure vertical plane. Circles correspond to 1 and 2 r.m.s. beam sizes. Units: 1 mm for the horizontal and 0.1 mrad for the vertical axis.*

that the beam spot is centered at the target. The trajectory correction and the required corrector strengths was the subject of an earlier study [9]. Without errors all particles (bunches) should reach the end of the line at the same spot. In Fig.6 we show an example of the distribution in phase space with all errors included, except angle and position errors at injection in the transfer line. The contours correspond to 1.0 and 2.0 σ_x and σ_y. The horizontal mean position is moved by 0.16 mm and the vertical by less than 0.02 mm. While the σ of the vertical distribution is very small, i.e. less than 0.01 mm, the horizontal σ is approximately 0.1 mm, being about 20% of the 1 σ beam size. Fig.7 shows the spots at the target for very large horizontal and vertical trajectories (misalignments increase tenfold). Obviously the position of the beam spot is largely displaced, the spot size is practically unchanged.

5.3 Effect of injection errors

The result of angle and positioning errors after extraction from the SPS (i.e. at injection into the proton beam line TT40-TT41) are first shown separately (Figs. 8 and 9) than for both together (Fig. 10). For the horizontal plane, it is clear that the spot size is dominated by these injection errors, provided they change from shot to shot and cannot be corrected or stabilized. The effective spot size is larger than 1 σ of the nominal beam size. Since the injection errors (angle and position) appear only in the horizontal plane, the vertical beam position is determined by trajectory errors and the spot size is not increased. Therefore in the vertical plane the beam appears as a displaced dot in the figures.

9

Type of error		Horizontal σ_x at target (mm)	Horizontal σ_x' at target (μrad)
Magnet (field and alignment) errors	see above	0.12 mm	11 μrad
Horizontal injection angle	10 μrad r.m.s.	0.11 mm	5 μrad
Horizontal injection position	0.5 mm r.m.s.	0.32 mm	21 μrad
Injection position and angle	see above	0.34 mm	21 μrad
Injection and magnet errors	see above	0.36 mm	22 μrad
Nominal beam size (r.m.s.)		0.53 mm	53 μrad
Effective total spot size (r.m.s.)		0.64 mm	57 μrad

Table 6: *Contribution of different errors to the beam stability and effective beam spot size on the target.*

5.4   Effect of all errors combined together

In the Fig.11 we show the spot size including all errors, i.e. the magnet field errors and misalignments as well as both types of injection errors. The findings are summarized in Tab.6. Although on first sight the spread of the beam position on the target looks large when all errors are included, the actual increase of the effective spot size on the target, i.e. when the beam size is folded with the fluctuation of the bunch centre, is modest and probably acceptable.
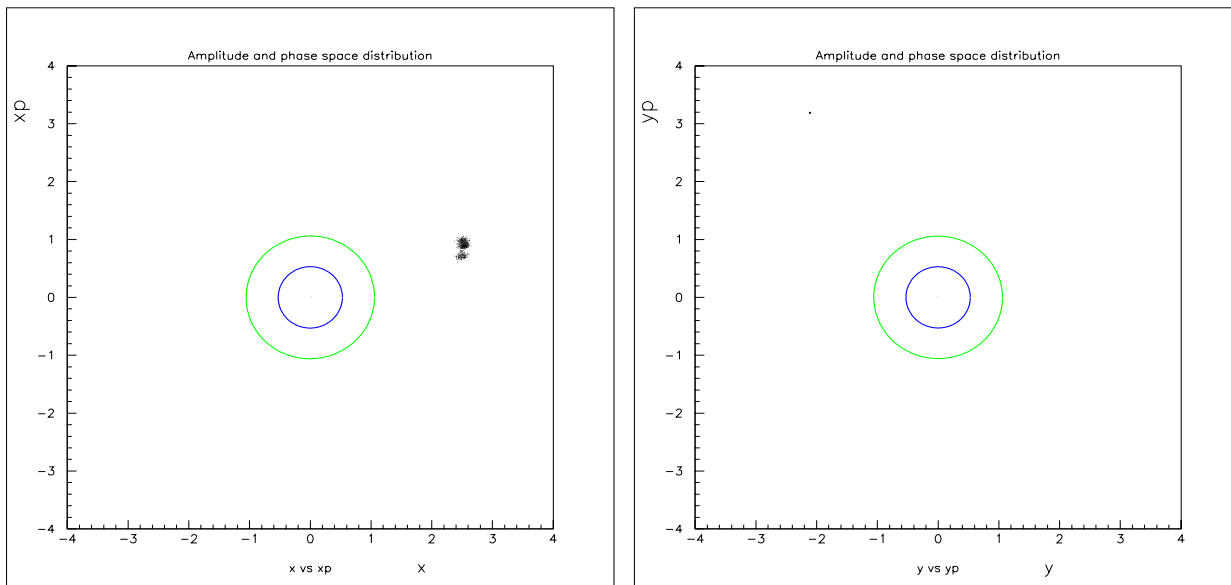
Figure 7: *Stability and beam spot at the target for an extreme trajectory (uncorrected). Left figure horizontal and right figure vertical plane. Circles correspond to 1 and 2 r.m.s. beam sizes. Units: 1 mm for the horizontal and 0.1 mrad for the vertical axis.*
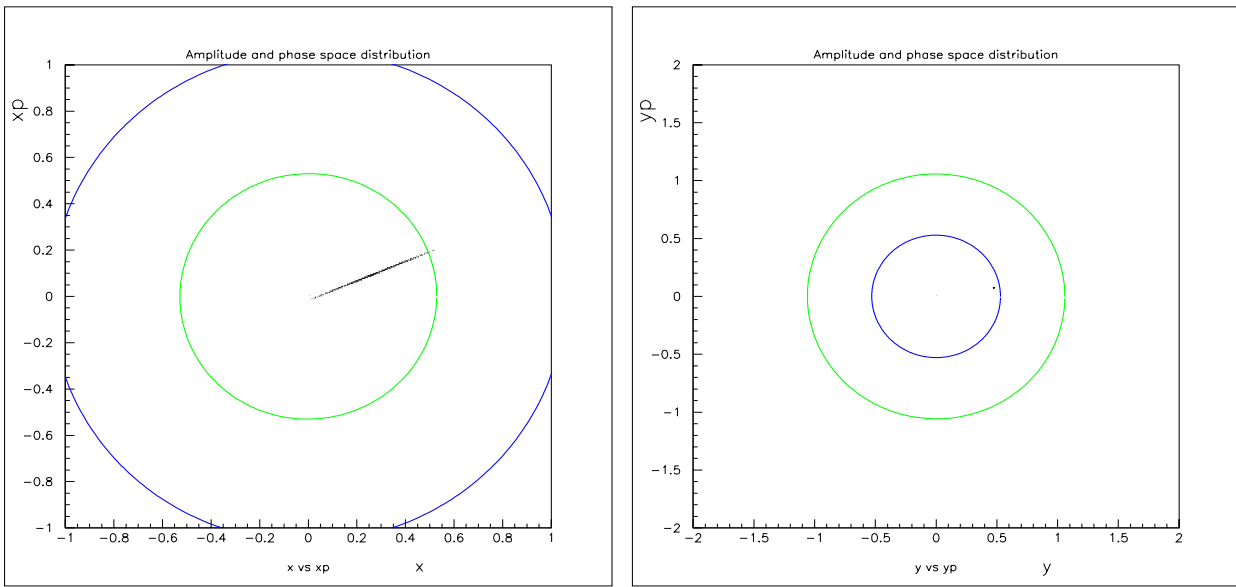
Figure 8: *Stability and beam spot at the target with angle error at injection. Left figure horizontal and right figure vertical plane. Units: 1 mm for the horizontal and 0.1 mrad for the vertical axis.*
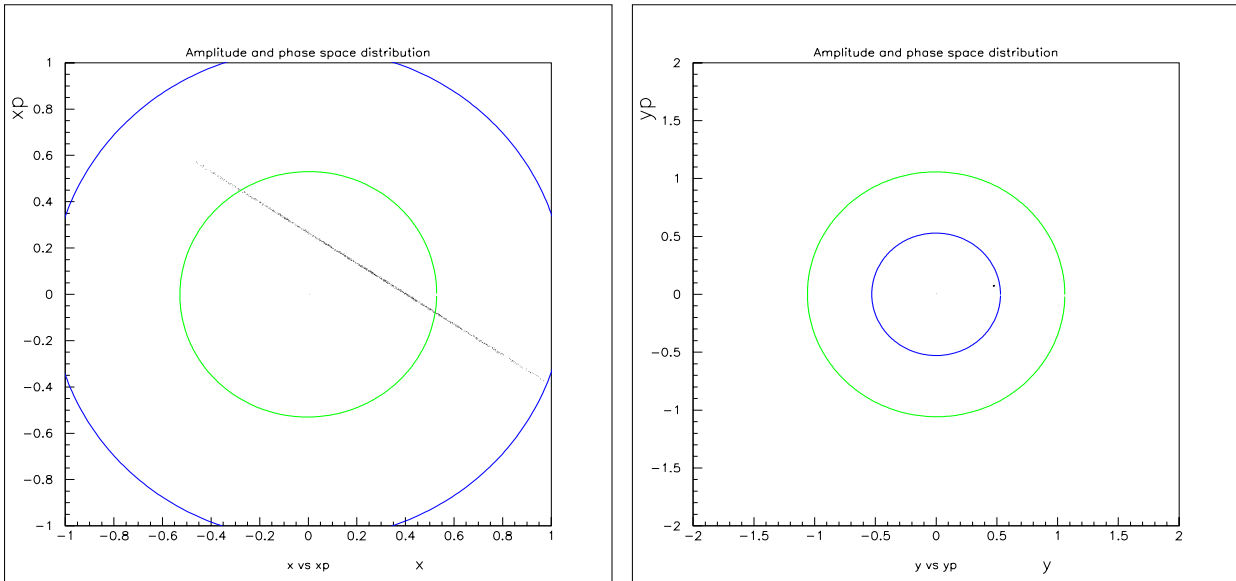
Figure 9: *Stability and beam spot at the target with position error at injection. Left figure horizontal and right figure vertical plane. Units: 1 mm for the horizontal and 0.1 mrad for the vertical axis.*

In principle, the errors also affect the aperture studied in a previous section. However, the changes in the beam size and amplitude are too small to be important, in particular for the already increased beam size used in the simulations.

6 Conclusions

Exploiting and testing extensively new features in the MAD-X program we have evaluated the available mechanical aperture in the proton beam line TT41 and established the possible bottlenecks of the aperture. We found that the aperture is according to the design and expectations. We have further inves-
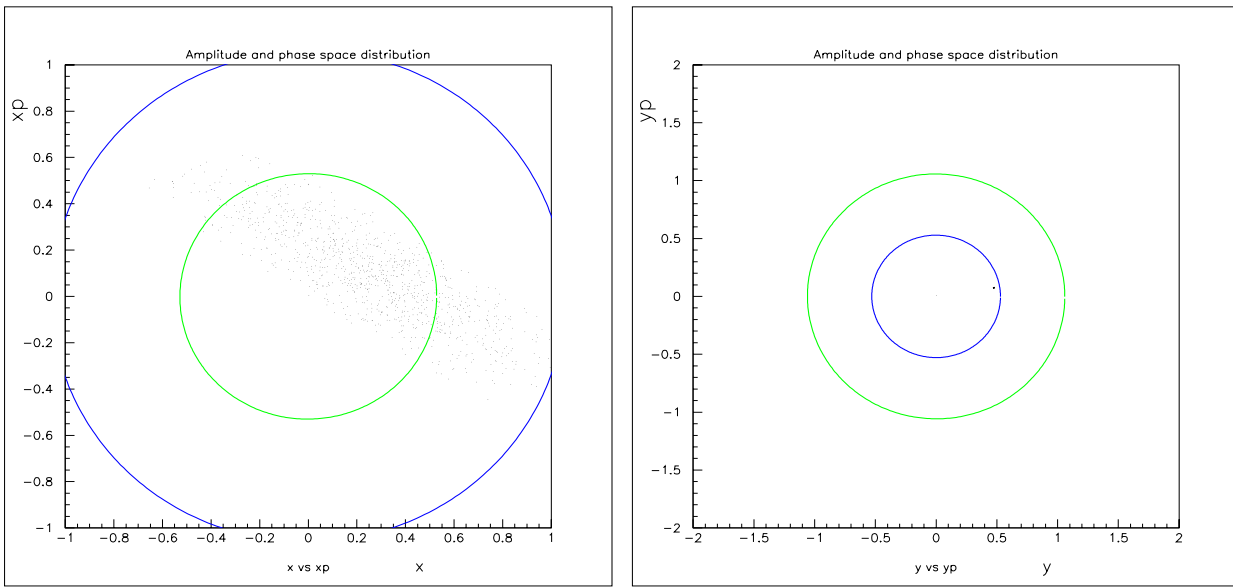
Figure 10: *Stability and beam spot at the target with angle and position error at injection. Left figure horizontal and right figure vertical plane. Units: 1 mm for the horizontal and 0.1 mrad for the vertical axis.*
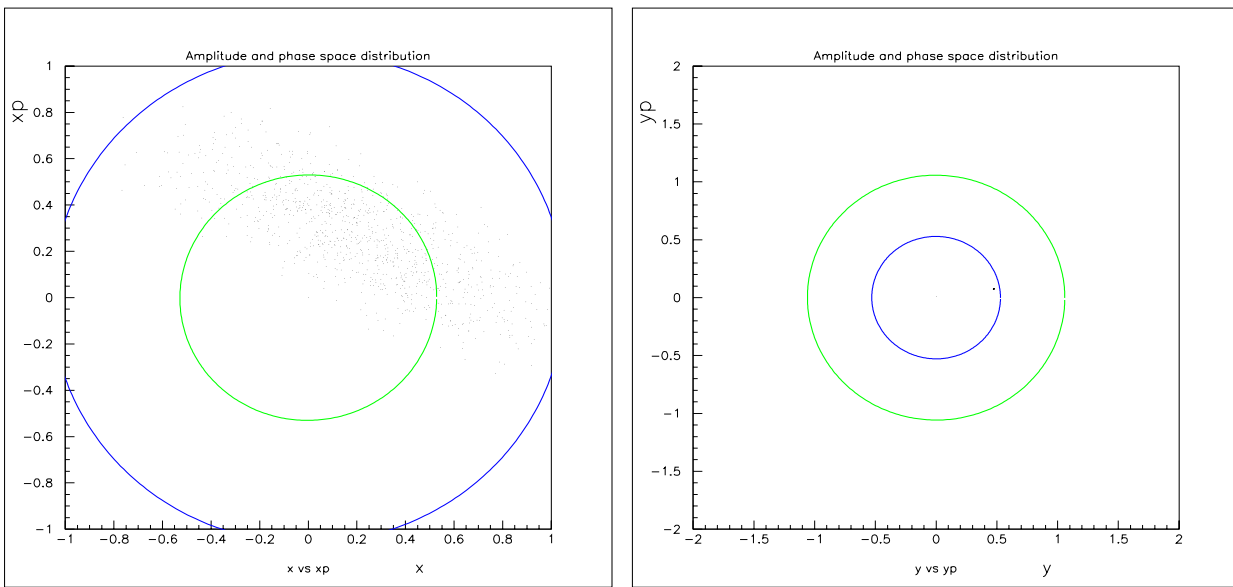
Figure 11: *Stability and beam spot at the target with magnet misalignment and field errors as well as injection errors (position and angle). Left figure horizontal and right figure vertical plane.*

tigated the stability of the beam spot on the target, simulating the expected imperfections of the beam line elements and including possible injection errors. The increase of the effective beam spot on the target is acceptable when these imperfections remain within their specifications.

References

[1] K. Elsener, editor; *The CERN neutrino beam to Gran Sasso*, Conceptual Technical Design, CERN 98-02, INFN/AE-98/05, 19 May 1998.

[2] *The CERN Neutrino beam to Gran Sasso (NGS)*, Addendum to report CERN 98-02, INFN/AE-98/05; CERN-SL/99-034(DI), INFN/AE-99/05.

[3] CNGS project team; *Update of changes to CNGS layout and parameters*, SL-Note-2002-012 EA.

[4] B. Goddard; *Fast extraction from SPS LSS4 for the LHC and NGS projects*, SL-Note-98-066 SLI.

[5] *The MKE Home Page, version April 2002*, $http://uythoven.home.cern.ch/uythoven/Html/MKE/MKE\_home.htm$.

[6] B. Goddard et al.; *The new SPS extraction channel for LHC and CNGS*, 2000 EPAC proceedings, Vienna, 26-30 June 2002 (2000), 2240 and CERN-SL-BT-2000-036-BT.

[7] J. Uythoven, E. Gaxiola, M. Timmins; *Upgrade of the SPS Extraction Kickers for LHC and CNGS Operation*, 2002 EPAC proceedings, Paris, 3-7 June 2002 and CERN-SL-2002-042 BT.

[8] *The MAD-X Home Page, version February 2003*, $http://frs.home.cern.ch/frs/Xdoc/mad-X.html$.

[9] W. Herr and M. Meddahi; *Trajectory Correction studies for the CNGS proton beam line*, SL-Note-2002-015 AP, May 2002.

[10] Best estimate for the momentum deviation from a private communication with G. Arduini and T. Bohl on 19 december 2002.

[11] B. Balhan et al.; *Alignment and girder position of MSE septa in the new LSS4 extraction channel in the SPS*, SL Note-2002-014-BT.

[12] K. Schirm; *Design report of the MBG main bending dipoles for the proton transfer line TT41 to CNGS*, SL-Note-2001-051 MS.

[13] T. Zickler; *Design report of the QTG quadrupoles for the CERN CNGS line*; SL-Note-2000-049 MS.